ORIGINAL RESEARCH

CrossMark

Development of a three-dimensional finite element method simulation model to predict modified flow drilling tool performance

Ekrem Oezkaya[1] · Stefan Hannich[1] · Dirk Biermann[1]

Abstract

Flow drilling is a relatively unexplored manufacturing process in which the tool penetrates the workpiece with a defined force or defined feed along its rotational axis. This paper presents a developed three-dimensional (3D)-finite element method (FEM) simulation model to predict the performance of modified flow drilling tools. To validate the simulation model, the flow drilling of AlSi10Mg with a non-pre-heated ($T_{initial} = 20$ °C) and pre-heated ($T_{influenced} = 200$ °C) tool was investigated. Thereby, the comparison of measured and simulated values of temperature, force and torques showed a good agreement. The comparison of the forces and torques concluded in almost identical maximum values. Nevertheless, the pre-heated tool was found to have a significantly more continuous heat distribution and higher bore quality than non-pre-heated flow drills, which can be attributed to the better formability of the cast aluminum alloy at elevated temperatures. Since the results of the simulation showed a good agreement with the experimental values, the three-dimensional model was used to predict the process behavior of a modified flow drilling tool, which could contribute to the optimization of the process. The result show, that the process time could be reduced by half, while the occurring temperatures, forces and torques remained acceptable.

Keywords Finite element method · Flow drilling · Heat exchange · 3D modeling · 3D FEM flow drilling simulation

Nomenclature

A	Initial yield N/mm^2
B	Hardening modulus
Cs	Strain rate sensitivity
c	Specific heat, J/(kg.K)
D	Cumulative-damage fracture factor
$d_1...d_5$	Damage constants
d_{FD}	Tool diameter, mm
d_2	Shrank diameter, mm
F	Force, N
h_{Cy}	Cylindrical height, mm
h_{Co}	Conical height, mm
h_T	Tip/center height, mm
k	Heat conductivity, W/(m.K)
l	Length, mm
l_t	Drilling depth (simulation), mm
M_t	Torque, Nm
m	Thermal softening effect
n	Rotational speed, 1/min
Rz	Average surface roughness
t	Time, s
T	Homogenous temperature, K
T_f	Friction moment, K
t_h	Thick, mm
$T_{influenced}$	Influenced temperature, °C
$T_{initial}$	Initial temperature, °C
T_m	Melting temperature, K
T_r	Transition temperature, K
v_c	Peripheral speed
v_f	Feed speed, mm/min
w	Wide, mm
$\dot{q}_f$	Heat generation, m/s

Greek symbols

α_{FD}	Tip/center angle, degree
ε_m	Emission rate
$\varepsilon_{plastic}$	Plastic strain
β_{FD}	Conical angle, degree
$\dot{\varepsilon}$	Strain rate, 1/s
$\dot{\varepsilon}_0$	Reference strain rate, 1/s
ε_f	Equivalent strain to fracture, 1/s

✉ Ekrem Oezkaya
oezkaya@isf.de

[1] Institute of Machining Technology, Technical University of Dortmund, 44227 Dortmund, Germany

$\dot{\varepsilon}_{pl}$	Comparative strain rate, 1/s
η	Hardening exponent
σ	Flow stress, N/mm^2
ρ	Density, N/m^2
ρ_h	Hydrostatic pressure, hPa
ω	Angular velocity, rad.s^{-1}

Abbreviations

Al	Aluminum alloy
approx.	Approximate
Bal.	Balance
Cu	Copper
DIN	German institute for standardization
3D	Three-dimensional
EN	European standards
FEM	Finite element method
FE	Finite element
Fe	Iron
Mg	Magnesium
Mn	Manganese
Ni	Nickel
Pb	Lead
Si	Silicon
Sn	Tin
Ti	Titanium
WC	Tungsten carbide
x, y, z	Cartesian coordinates
Zn	Zinc

Introduction

Flow drilling is a chipless manufacturing process used to produce bores in relatively thin-walled tubes or bushes and is also known as thermal drilling, plastic drilling, thermoplastic drilling, form drilling and friction stir drilling [1]. Only few studies exist on the flow drilling process [2]. For machining of thin-walled profiles, the mechanical loads acting on the workpiece are of special interest, since elastic and plastic deformations could influence the integrity of the workpiece [3]. A major industrial application of flow drilling is the manufacturing of bushings for high-strength threads in thin-walled plates, tubes or tube profiles. Subsequently manufactured threads by chipless processes such as thread-forming show a particularly high pull-out strength [4].

During flow drilling, the rotating tool is positioned in front of the workpiece and then moved along the tool axis under high axial pressure and high speed to achieve an adequate temperature [5]. The occurring frictional heat between tool and workpiece decreases the material strength, resulting in good formability and penetration. Tool temperatures up to $T = 900$ °C and workpiece temperatures about $T = 700$ °C occur [6]. An important parameter for good ductility when flow drilling is the ratio between workpiece thickness and tool diameter depending on the thermal conductivity coefficient [7]. A small amount of lubricant is used in exceptional cases to avoid material transfer or adhering of the workpiece material on the tool surface [8]. The tools are generally made out of specially sintered carbide grades to satisfy the high requirements regarding wear resistance, hardness and temperature resistance. Therefore carbide tools are especially suitable for flow drilling [9]. The geometry of the flow drill can be divided into a center region, conical region, cylindrical region, shoulder region und shank region (Fig. 1). The center and conical region widen the bore. Subsequently the cylindrical region creates the actual workpiece form and defines the surface quality. Upward extruded material can be machined or formed regarding to the application of the tool collar [10]. The shank region is used for tool mounting. Amongst other aspects, the mechanical process is described in [11].

The physical processes during flow drilling involve friction and extrusion, while the material is subjected to intense heating and deformation, which affects the microstructure [1]. Flow drilling can be successfully applied on many different materials. Aluminum alloys ensure a high degree of
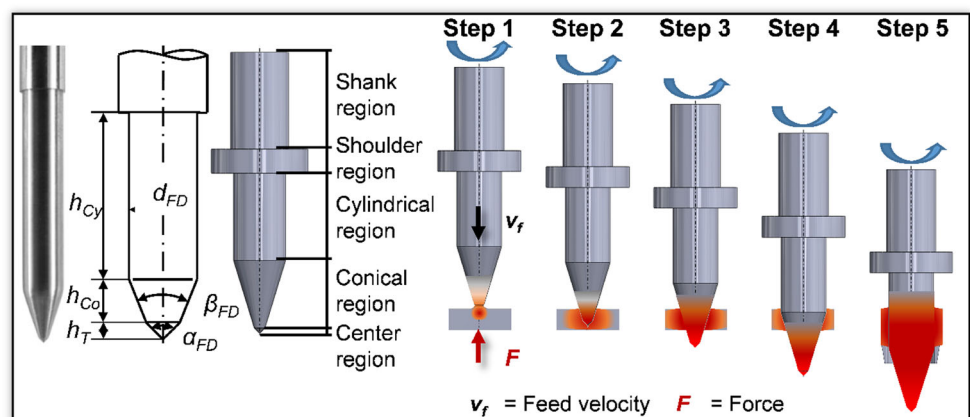

Fig. 1 Stages of flow drilling

Table 1 Chemical composition of AlSi10Mg alloy (wt.-%)

	Al	Mg	Si	Fe	Cu	Mn	Ni	Zn	Pb	Sn	Ti	Others
DIN EN 1706	Bal.	0.2–0.45	9–11	<0.55	<0.05	<0.45	<0.05	<0.1	<0.05	<0.05	<0.15	<0.15
AlSi10Mg	Bal.	0.34	9.4	0.16	0.01	0.04	0.003	0.02	0.001	0.01	0.11	0.01

stiffness with a minimum weight and are therefore used in many areas of technical engineering, especially in the automotive industry [12, 13].

In the presented work a 3D FEM simulation model was developed, which could be used to optimize the flow drilling process by modifying the tool geometry and analyzing the according impact on process parameters like temperatures, forces and torques. The flow drilling process is investigated on the aluminum cast alloy AlSi10Mg. The low formability of this material class complicates performing flow drilling without any process adjustments. Because of this, a pre-heating of the tool was applied. For tempering the tool, inductive heating, heating by radiation of halogen incandescent ceramic heating elements and direct resistance heating can be used. Induction heating systems are widely spread for heating up metallic materials and were also used in this work [14]. Since the feed rate during flow drilling is determined by the rotation frequency, the process is similar to the principle of regular machining processes. The three-dimensional modelling and FEM simulation, which have already become established for machining processes [15–17], come with certain challenges for flow drilling, since it is still a relatively unexplored manufacturing process. The flow drilling was carried out with two different initial tool temperatures (20 °C / 200 °C) and the simulation results were compared to experimentally obtained data. Based on this, the simulation model was used to predict the performance of a modified tool, whereby it could be found, that the process time could be significantly reduced compared to the standard tool.

Experimental setup

The presented work deals with the analysis of flow drilling of the aluminum cast alloy AlSi10Mg. The low formability of this alloy complicates the flow drilling without any process adjustments. In the following chapter, the material properties

Fig. 2 Measuring instruments

Thermographic measurement
Thermographic camera
Software

Measurement platform
Software

Induction heating
Machine vice | Inductor | Tool
IR-pyrometer
Measuring device
Workpiece

Process device: Induction heating
Capacity:	2000 W
Frequency:	0.25 – 0.55 MHz
Measuring range of pyrometer:	150°C – 750°C
Spectral range:	2.1 μm
Control interval:	2 ms

Measuring device: Thermographic camera
Resolution:	640 x 512 pixels
Frame rate:	80 pic./second
Spectral range:	2–5 μm

Measuring device : Measurement platform
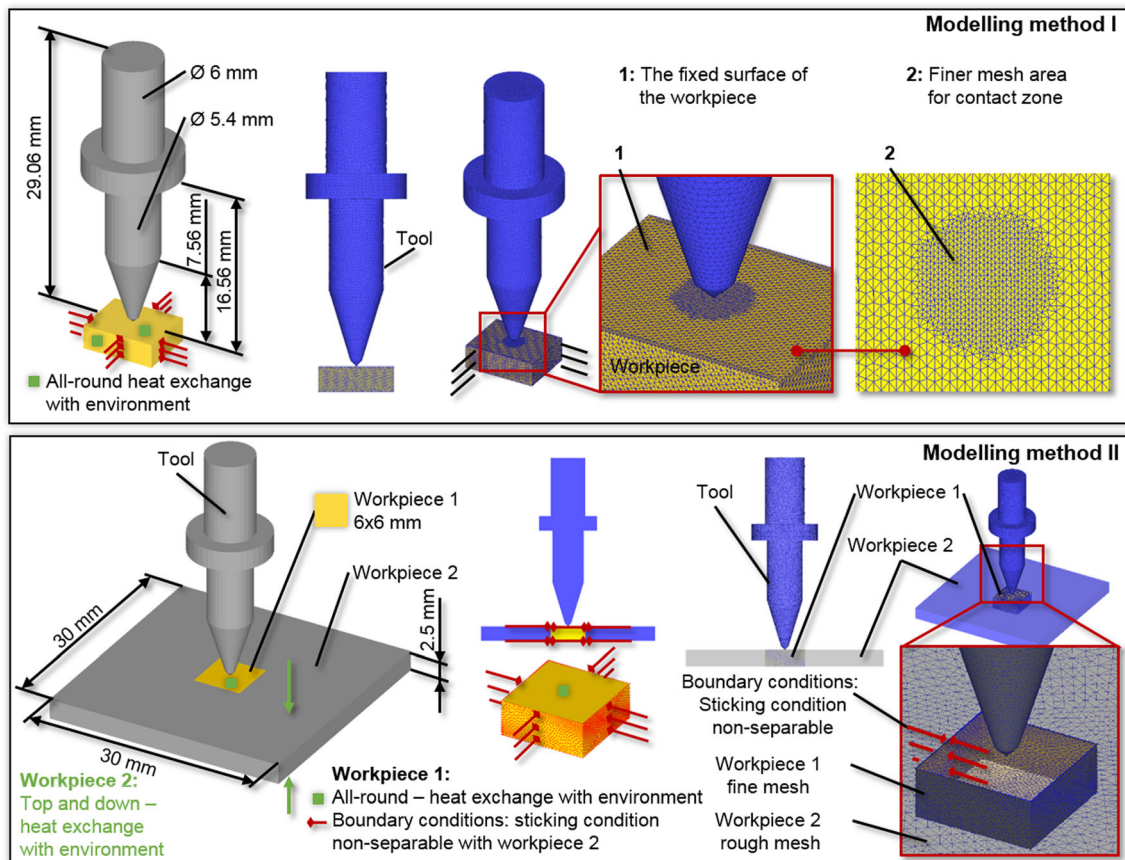| Platform type: | Kistler 9255B |
| Measuring range: | F_z = -10k–60kN |
| Responsiveness: | <0,01 N |

Fig. 3 Developed model for the 3D FEM flow drilling simulation

and the experimental setup with its measuring and controlling devices as well as the drilling parameters will be described.

Material

In order to get exact information about the chemical composition of the used AlSi10Mg alloy, an optical emission spectroscopy has been conducted. The results and the related limiting values for alloying elements according to DIN EN 1706 are given in Table 1.

Experimental setup and process parameters

The experimental setup with its different devices is depicted in Fig. 2. All experiments were conducted on a GROB BZ 40 CS machining center. In order to measure the temperatures occurring during the flow drilling experiments, a high-speed thermographic camera of the type ImageIR 8300 from Infratec with a detector-resolution of 640×512 pixels was used. To ensure the possibility of recording the temperature development during the process, a frame rate of 80 pictures per second was used. The surface of the workpiece was blackened with a special varnish to get a high emission rate of $\varepsilon_m = 0.95$. The camera was positioned in such a way, that it was possible to

focus vertically on the side of the specimen. In order to measure temperatures as close to reality as possible, the bores in these experimental tests were set flush with the edge of the workpiece, which corresponds to a distance of $d = 2.7$ mm to the tool center point.

Table 2 Simulation parameters for method I and method II

	Method I	Method II
Tip/center angle	$\alpha_{FD} = 90°$	
Conical angle	$\beta_{FD} = 34°$	
Tool diameter	$d_{FD} = 5.4$ mm	
Shank diameter	$d_2 = 6$ mm	
Conical height	$h_{Co} = 7$ mm	
Drilling depth for simulation	$l_t = 10.5$ mm	
Workpiece material	AlSi10Mg	
Tool material	WC	
Material model	Johnson and Cook	
Workpiece 1 mesh elements	90,000	60,000
Workpiece 2 mesh elements	–	50,000
Tool mesh elements	100,000	
Computing time	approx. 720 h	approx. 168 h

Table 3 Used parameters for Johnson and Cook model

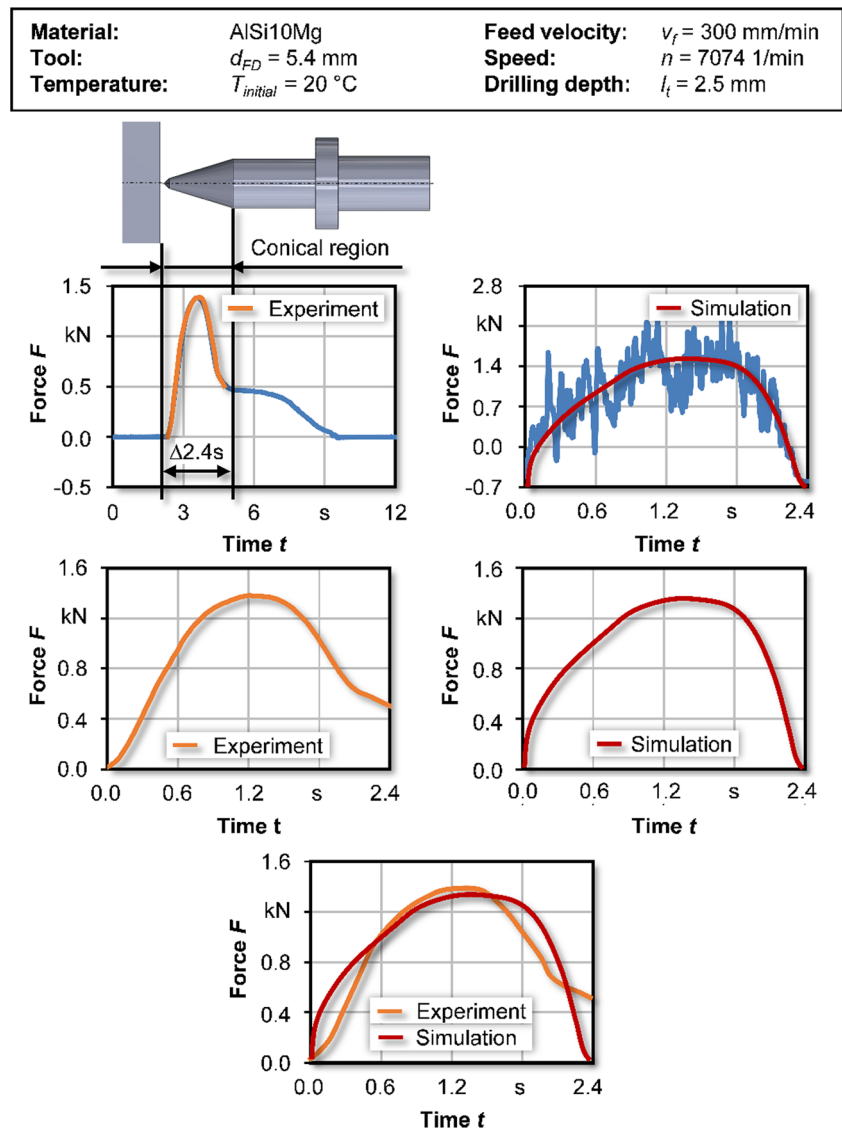| A in MPa	B in MPa	η	C_S	$\dot{\varepsilon}_0$ in 1/s	m	T_r in K	T_m in K
270	155	0.28	0.018	0.001	1.43	293.15	830.15

During the experiments, a pre-heating of the tool was applied in order to improve the formability of the aluminum cast alloy. In this study, a portable induction system of the type Himmelwerk HU2000 Plus was used. As depicted in Fig. 2, the inductor was placed near the machine vice within the machine room. An IR-pyrometer as well as a contact thermometer were assembled to control the initial tool temperatures.

Another aspect in the validation of the simulative results are the mechanical loads. In order to measure the feed forces and torques during the experiments, a piezo-electric-measuring-platform type 9255B and a charge amplifier type 5070 from Kistler were used. The measured data was analyzed with the software DIAdem.

The general design of flow drilling tools was already described in chapter 1. Tools used in this study are solid carbide tools without coating. All tools have a diameter of $d_{FD} = 5.4$ mm. The tool tip has a tip angle of $\alpha_{FD} = 90°$ and is the shortest part with a height of $h_T = 0.56$ mm in feed direction. The conical region is located after the tip and is constructed with a conical angle of $\beta_{FD} = 34°$. The height of the conical part measures $h_{Co} = 7$ mm. Following the conical region, the cylindrical part of the tool is located.

Fig. 4 Force validation with initial tool temperature of $T_{initial} = 20\ °C$

| Material:	AlSi10Mg	Feed velocity:	v_f = 300 mm/min
Tool:	d_{FD} = 5.4 mm	**Speed:**	n = 7074 1/min
Temperature:	$T_{initial}$ = 20 °C	**Drilling depth:**	l_t = 2.5 mm

To validate the numerically calculated forces and torques, experiments with the same process parameters were conducted. The peripheral speed was set to $v_c = 120$ m/min and the feed velocity was adjusted to $v_f = 300$ mm/min. The experiments as well as the simulations were carried out with to different initial tool temperatures. In a first step, no pre-heating of the tool was used, which lead to a tool temperature of $T_{initial} = 20$ °C. In order to improve the formability of AlSi10Mg and to reduce the mechanical loads, a pre-heating to $T_{influenced} = 200$ °C was realized. Multiple friction drilled bores were done on a larger sample. Sample dimensions were 80×50 mm. The distance between the bore middle points was 15 mm. After every bore, it was waited until the tool and the workpiece returned to room temperature again.

Development of an 3D FEM simulation model for flow drilling

The finite element modelling (FEM) is an established tool for the analysis of machining and forming processes. It helps to reduce the extensive experiments and to understand and optimize these operations. For this simulation, the FEM software DEFORM 3D and the adaptive mesh technique of the Arbitrary Lagrangian Eulerian method were used, which does not alter the topology of the mesh. With the adaptive meshing technique, the element nodes adapt independently of the material in order to prevent strong element deformation. The ALE method combines the advantages of the Lagrangian and the Euler formulation, i.e. it reduces mesh distortion while correctly mapping the boundary conditions.

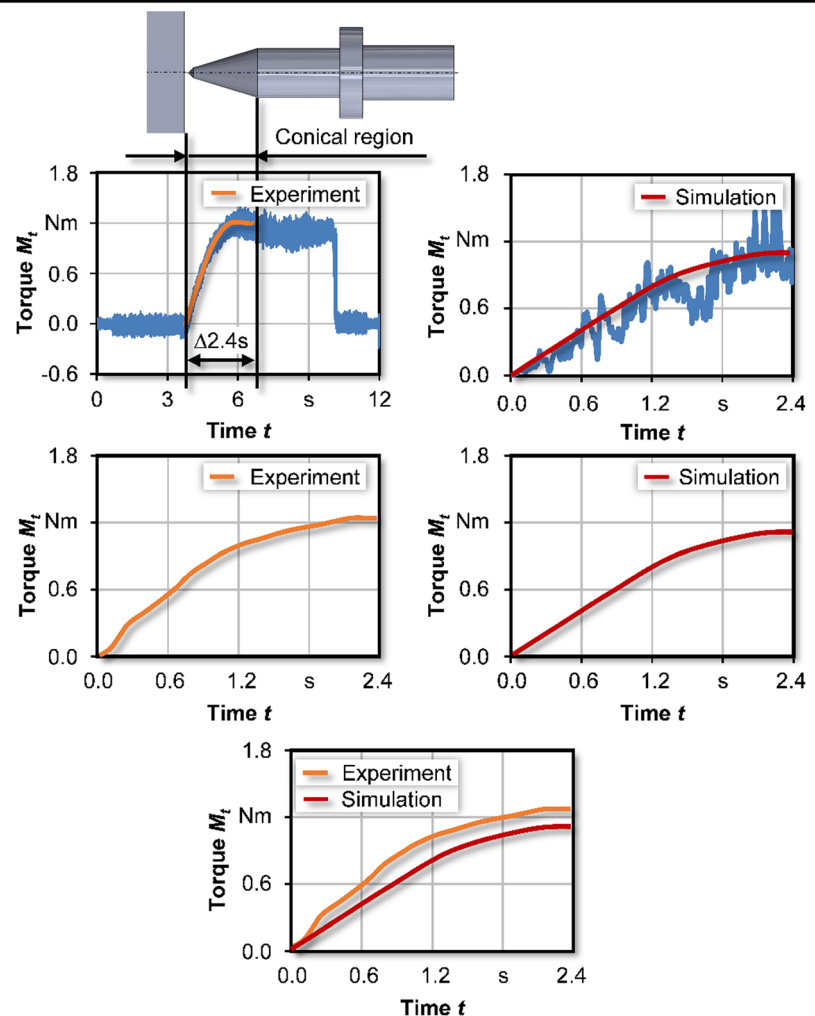**Fig. 5** Force validation with initial tool temperature of $T_{influenced} = 200$ °C
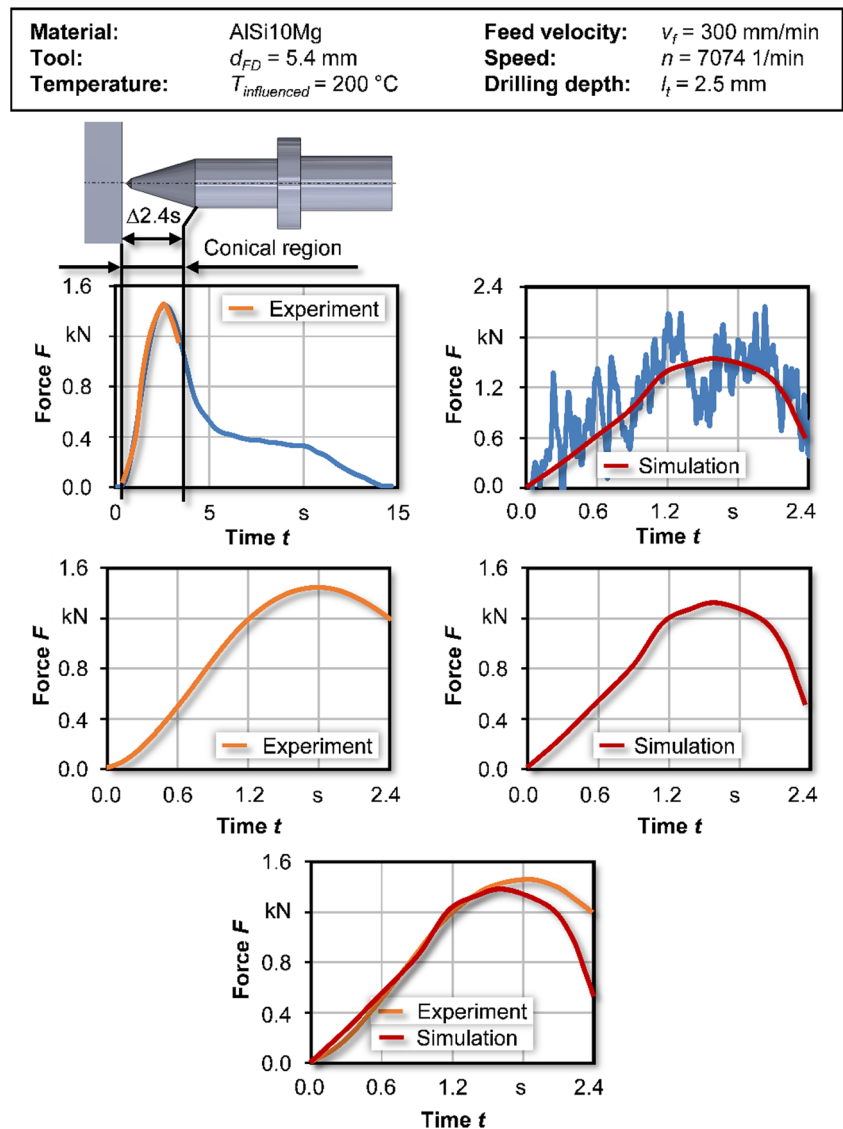
The three-dimensional FE modelling was carried out using two different methods I and II. The method I was intended to achieve the shortest possible computing time by minimizing the workpiece dimensions (Fig. 3). With this model, heat exchange with the environment after the tool penetrated the workpiece was limited by the small dimensions and only possible via the upper and lower workpiece surfaces. However, as the results in chapter 4 show, the forming process leads to a heat accumulation on all six surfaces of the workpiece. For this reason, a further method II was implemented to enable heat exchange with the environment via all six surfaces. A second workpiece was added to fix the original workpiece 1 with the non-separable condition in all special directions of the workpiece 2 (l = 30 x w = 30 mm). Thereby, the heat accumulation could be prevented, so that the flow drilling process could be reproduced realistically.

The meshing procedure, which differs for the methods I and II. In both cases, the orientation of the tool axis to the workpiece surface is rectangular and the contact surface is symmetrical. For method I, the contact zone between tool and workpiece, where the tool penetrates the material, was selected for a local meshing procedure with very fine tetrahedral elements. These smaller finite elements are especially necessary in places where large stress gradients are expected, since otherwise inaccurate results could occur. However, due to the small dimensioning, the numerical calculation could not be carried out completely, since the mesh nodes of the workpiece side surfaces could not be deformed any further, which ultimately led to a heat accumulation. In method II, the fixed workpiece 1, where the actual penetration takes place, was discretized with fine tetrahedron elements and the workpiece 2, which prevents heat accumulation, was meshed with rougher tetrahedron elements. This approach provided the possibility to deform the former problematic mesh nodes in all directions, so that tool and workpiece behavior could be modelled realistically for the performed simulation. Detailed

Fig. 6 Torque validation with initial tool temperature of $T_{initial}$ = 20 °C

information on the mesh settings and simulation parameters are listed in Table 2.

The heat generation during flow drilling is influenced by the plastic energy loss due to the shear deformation and the friction between the tool and the workpiece, whereby the latter accounts for 98 to 99% of the total heat generation [18]. The heat transfer that occurs during the penetration can be described as:

$$\rho c = \frac{\partial T}{\partial t} = \left[k_x \frac{\partial^2 T}{\partial x^2} + k_y \frac{\partial^2 T}{\partial y^2} + \frac{\partial^2 T}{\partial z^2} \right] + \dot{q}_f \qquad (1)$$

whereby T is the temperature, ρ the material density, t the time, k the heat conductivity, c the specific heat in all three Cartesian coordinates, while $\dot{q}_f$ describes the heat generation generated by friction.

The heat generated by friction is the result of the integral over the angular velocity of the tool ω in the interval of the friction moment in the contact zone T_f and 0:

$$\int_0^{T_f} \omega \ dT. \qquad (2)$$

In current literature, relatively thin tool plates are used for FEM simulations. In the simulation performed here, the bore was drilled into a $t_h = 2.5$ mm thick workpiece plate, which led to convergence problems in the numerical calculation. Only the use of the specific material parameters A (initial yield), B (hardening modulus), $\varepsilon_{plastic}$ (plastic strain), C_S (strain rate sensitivity), η (hardening exponent), m (thermal softening effect) and $\dot{\varepsilon}_0$ (reference strain rate), T (homogenous temperature), T_r (transition temperature) and T_m (melting temperature) for the aluminum cast alloy in the Johnson and Cook model (Eq.

Fig. 7 Torque validation with initial tool temperature of $T_{influenced} = 200$ °C
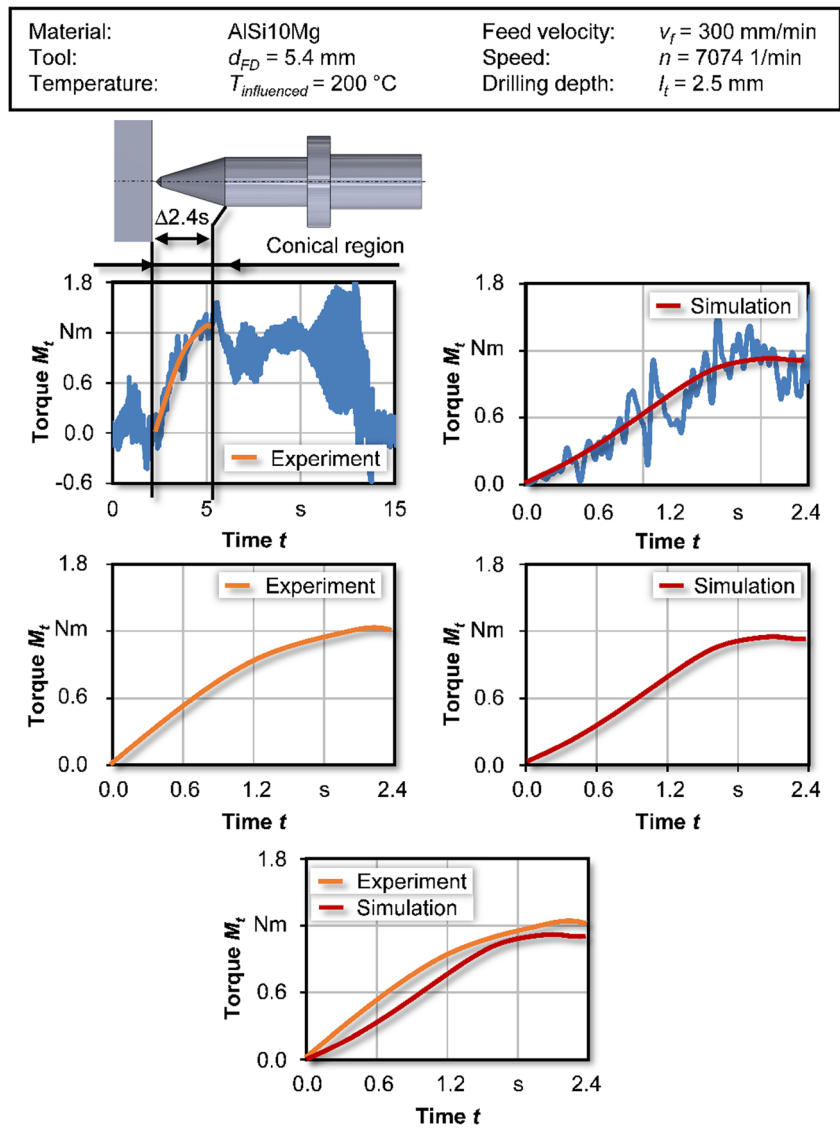
3) resulted in a good mesh quality and convergence (Table 3) [19]:

$$\sigma = \left(A + B\varepsilon_{plastic}^{\eta}\right)\left[1 + C_s \cdot \ln\left(\frac{\dot{\varepsilon}}{\dot{\varepsilon}_0}\right)\right]\left[1 - \left(\frac{T-T_r}{T_m-T_r}\right)^m\right]. \quad (3)$$

Results and validation of modelling method II

Feed forces at initial tool temperatures of 20 °C and 200 °C

Besides the temperature development, the numerically calculated forces and torques were compared to the experimentally measured values in order to validate the simulation results. As in the validation of the temperature development, the area from the center to the end of the conical region of the tool was examined. Analyzing the forces, an intense rise can be noticed as the tool starts to penetrate the workpiece due to the low heat generated by friction and the resulting higher material resistance. As the heat input increases, the flow resistance decreases in the effective zone and tool can penetrate the workpiece more easily. The heating reaches its maximum in the effective zone. Figures 4 and 5 shows that the actual deformation work is carried out in the first $t = 2.4$ s of the process. Therefore, the simulation results were validated with the experimental values in this time frame and show a good correlation. Analyzing the results without a pre-heating maximal forces of approx. $F = 1.3$ kN are reached in both, the simulation and experiments. Using a pre-heating of the tool to $T_{influenced} = 200$ °C the maximal forces show no significant difference to those without using a pre-heating.

Torque at initial tool temperatures of 20 °C and 200 °C

The torque follows a nearly linear course until the bore diameter is formed by the conical part of the tool and forms a plateau until the tool penetrates the workpiece. In this range, the torque remains constant, so that the $t = 2.4$ s time interval was taken into account for validating the simulation results
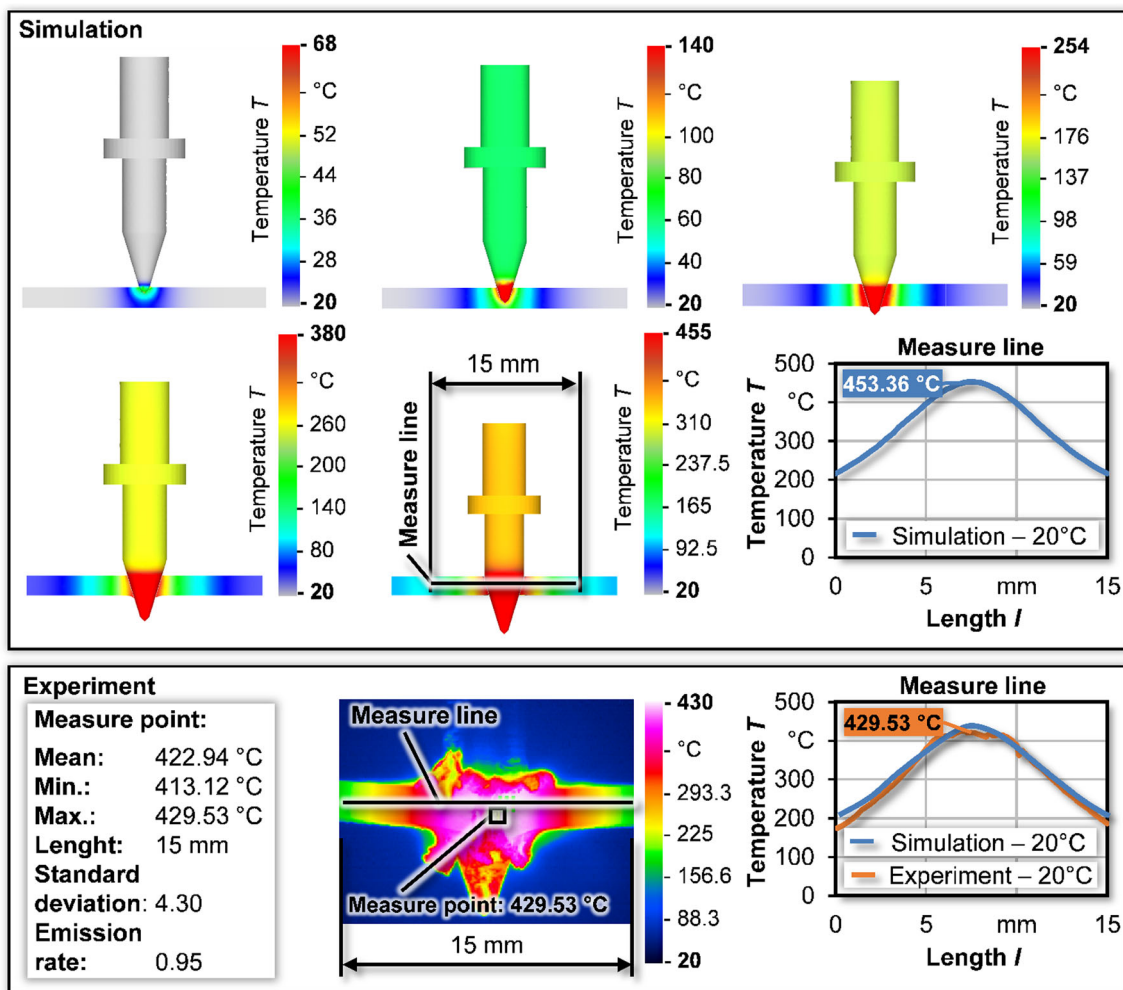

Fig. 8 Temperature development during the flow drilling process with initial tool temperature of $T_{initial} = 20$ °C
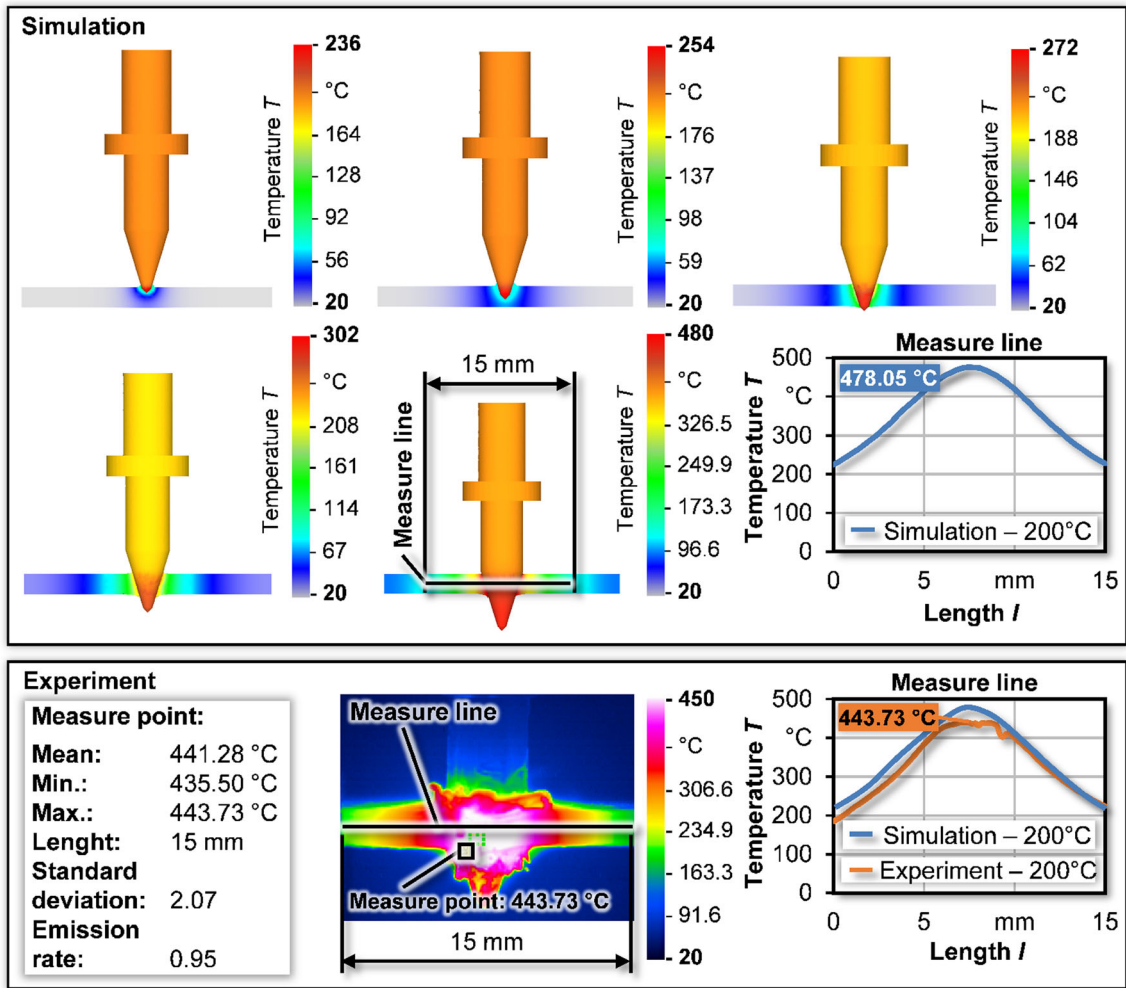
Fig. 9 Temperature development during the flow drilling process with initial tool temperature of $T_{influenced} = 200\ °C$
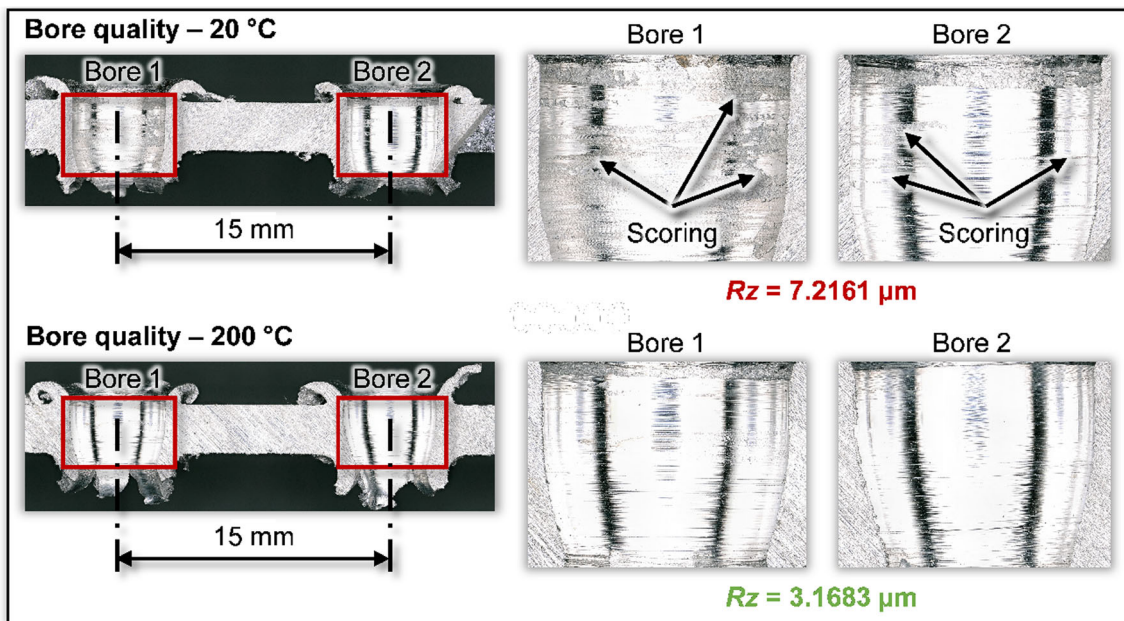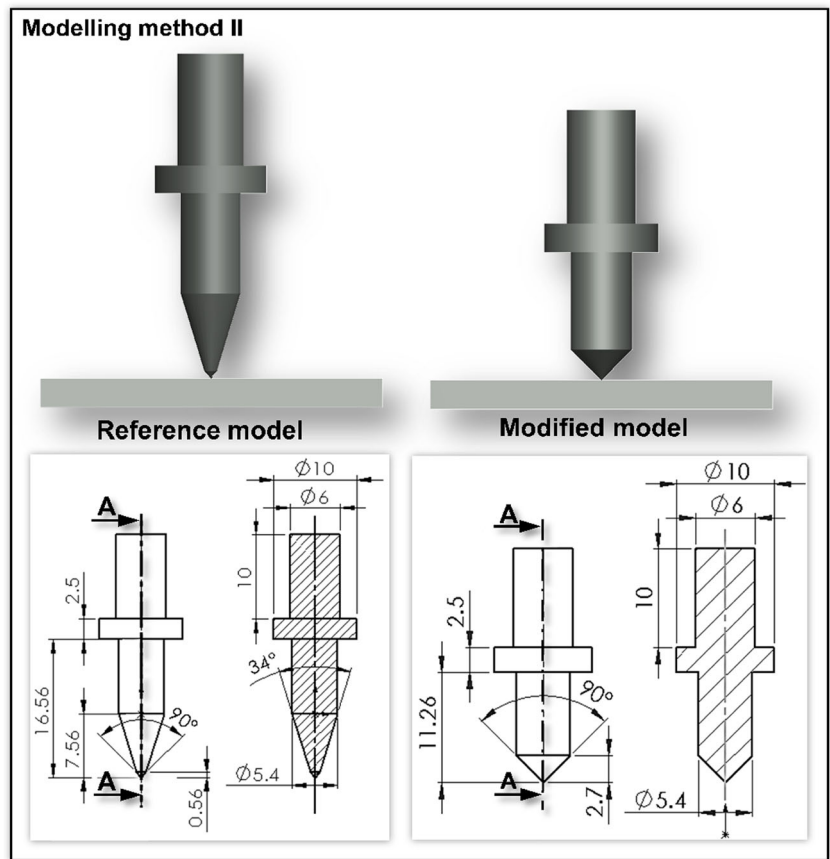

Fig. 10 Quality of the bore walls regarding the tool temperature

Fig. 11 Modified flow drill

(Figs. 6 and 7). As depicted, the simulated values show a good agreement with the experimentally determined torques. Maximal torques of approx. $M_t = 1.3$ Nm are reached without as well as with a pre-heated tool.

Heat exchange at initial tool temperatures of 20 °C and 200 °C

Figure 8 shows the heat exchange at an initial tool temperature of $T_{initial} = 20$ °C. The temperature rises continuously with increasing drilling depth and reaches a maximum of approx. $T = 453$ °C as the conical part of the tool is fully immerged into the workpiece. The maximum temperatures can be observed in this area of the process, as most forming work has to be carried out. The temperatures during the experimental tests, recorded with a thermographic camera, show corresponding results. The measured temperatures reach a maximum of approx. $T = 430$ °C. Furthermore, the temperature distribution along a measurement line can be analyzed. As depicted, simulative and experimental results show a good correlation.

According to Hutchinsona et al., the behavior of magnesium alloys changes considerably with increasing
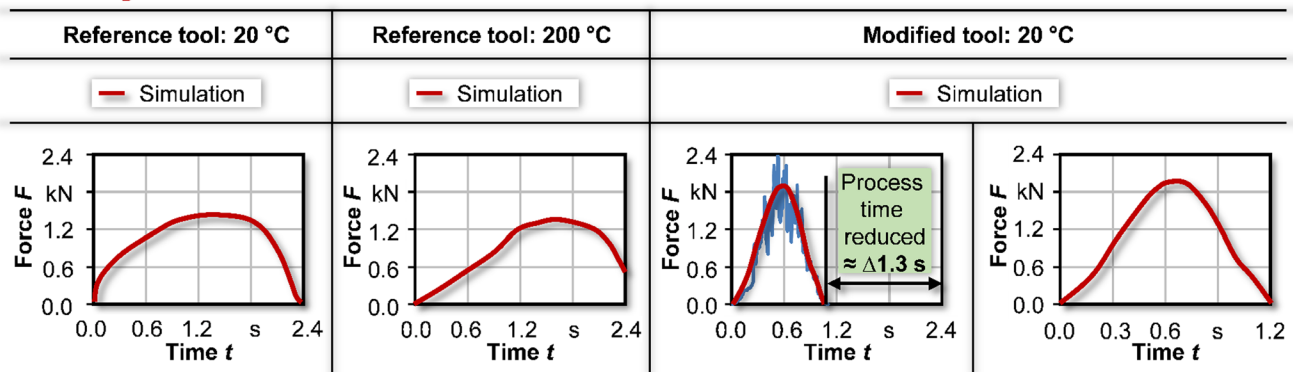

Fig. 12 Comparison of feed forces between the two reference simulations and the modified model

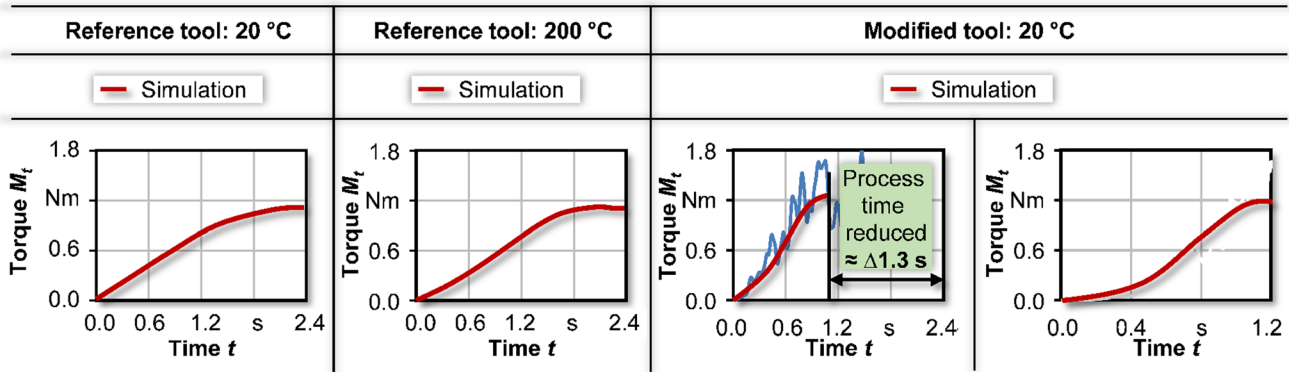**Modelling method II – torque**

Fig. 13 Comparison of torques between the two reference simulations and the modified model

temperatures, so that the ductility increases with the usual decrease in flow stress at temperature above $T_{influenced} = 200\ °C$ [20]. Similar effects can be used to improve the formability of aluminum alloys [21]. This way, the center region of the flow drilling tool penetrates the material more easily. Another advantage results in the improvement of the bore quality as shown in chapter 4.4. Figure 9 shows the temperature development during the flow drilling process with an influenced tool temperature of $T_{influenced} = 200\ °C$. Both the simulative and experimental results regarding maximum temperatures show a slight increase compared to the temperatures without pre-heated tools. The simulation results in a maximum temperature of approx. $T = 478\ °C$, whereas in the experimental tests a temperature of approx. $T = 444\ °C$ was measured. Based on these results, the simulation approach can be validated with respect to the temperature development during flow drilling.

Bore quality

The resulting bore quality is an important aspect in the evaluation of flow drilled bores. The low formability of aluminum cast alloys at room temperature makes it difficult to realize flow drilling without any process adjustments. For this reason,

the flow drilling tools were pre-heated via a portable induction system. In Fig. 10 the quality of the bore walls is depicted regarding the initial tool temperatures. Bores generated without a pre-heating of the tool showed a poor surface quality of the bore wall, which is dominated by relatively deep grooves. In contrast, a significant improvement in bore quality can be observed when pre-heating the tool to $T_{influenced} = 200\ °C$. Measurements of the surface roughness were carried out via a tactile measuring machine of the type MarSurf XR20. Using no pre-heating, the average surface roughness reached values of $Rz = 7.2161\ \mu m$, while using a pre-heating values of $Rz = 3.1683\ \mu m$ were measured. Since a higher tool temperature evidently increases the bore hole quality, while a pre-heating increases the process time and cost, according optimizations need to be carried out. The bore quality can effect a subsequent threading operation or the resulting characteristics of the threads, so that grooves have to be avoided in order to generate solid and stabile threads.

Flow drill modification and optimization

Based on the validated simulation model, the costs of tool development processes and uncertainties about possible
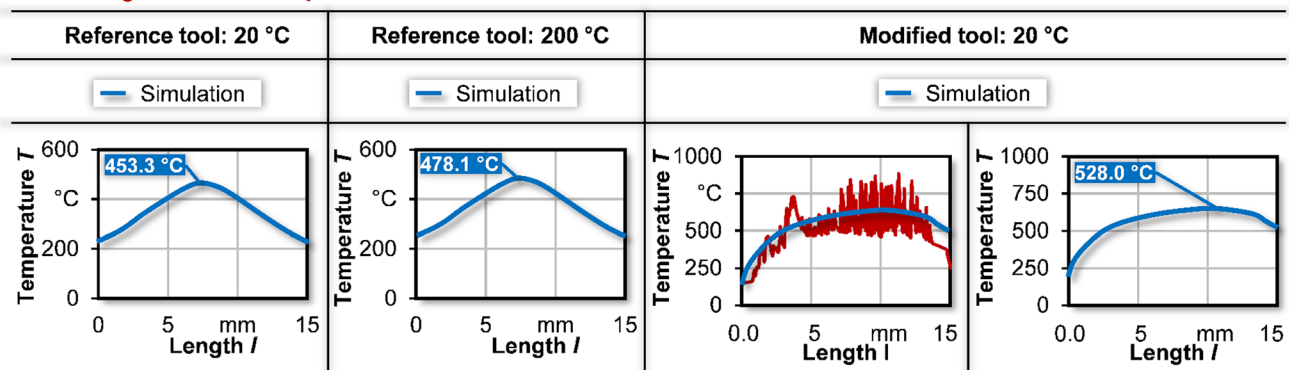
Modelling method II – temperature

Fig. 14 Comparison of temperatures between the two reference simulations and the modified model

design variations could be reduced by predicting feed force, torque and temperature in advance of experimental prototype production. Therefore, the flow drill was constructively modified by significantly shortening the conical region compared to the reference model (Fig. 11). The simulation was then carried out with the described modelling method II at a tool temperature of $T_{initial} = 20$ °C.

Results: Feed force of the modified flow drill

To evaluate the simulation of the modified tool, the resulting feed forces were compared to the validated reference tool with the two different initial tool temperatures (Fig. 12). It can be seen, that the feed force occurring during tool penetration is higher in comparison to the reference flow drilling tool, which is due to the modified shorter conical region and the resulting larger contact area between tool and workpiece. However, the process time is reduced by almost 50%, due to the shorter conical region.

Results: Torque of the modified flow drill

The torque of the modified tool is at a slightly higher level than that of the two reference simulations (Fig. 13). The contact surface between the tool and the workpiece increases quicker due to the modification, whereby the torque increases sharply for a short time. Compared to the two reference models, the torque plateau is achieved twice as fast with the modified tool.

Results: Temperature of the modified flow drill

The temperature occurring during the flow drilling process shows a much faster rise for the modified tool compared to both reference models (Fig. 14). The result indicates, that a considerably better flow behaviour could be achieved with the shortening of the conical region, due to the increased rise in temperature, resulting in better bore hole quality, as pointed out in chapter 4.4. In this context, it should again be mentioned that the process time could be reduced significantly, therefore benefitting for industrial applications.

Conclusion

This paper presented the development of a 3D FEM simulation model, which can be used to predict the modified flow drill behaviour. In this way, occurring feed force, torque and temperature can be analyzed before the production of expensive modified tool prototypes, thus reducing development time and development costs. With the first modelling method, the limited dimension of the workpiece led to heat accumulation, while the deformation could not be accurately displayed

due to the high mesh distortion. In order to model heat exchange with the environment in all directions, the workpiece dimensions were increased in the second modelling method and the FEM simulations were carried out on this basis. The simulated temperature development, forces and torques were compared and validated with experimental values. The simulation results showed that the flow drilling process can be simulated realistically, so that the developed simulation model was used to predict the process behavior of a modified flow drilling tool. The conical region of the flow drill model was shorted significantly compared to the reference model, so that the contact area between the tool and workpiece and in this context the friction area was enlarged. The results show that the feed force and torque reach a slightly higher level than the non-pre-heated and pre-heated (20 °C / 200 °C) reference models. Due to the increased friction area, the temperature rises faster and further. As a result, a better bore hole quality and shorter process time could be achieved with the modified tool geometry.

Compliance with ethical standards

Conflict of interest The authors declare that they have no conflict of interest.

Publisher's Note Springer Nature remains neutral with regard to jurisdictional claims in published maps and institutional affiliations.

References

1. Eliseev AA, Fortuna SV, Kolubaev EA, Kalashnikova TA (2017) Microstructure modification of 2024 aluminum alloy produced by friction drilling. Mater Sci Eng 691:121–125. https://doi.org/10.1016/j.msea.2017.03.040

2. Bilgin MB, Gök K, Gök A (2015) Three-dimensional finite element model of friction drilling process in hot forming processes. P I Mech Eng B-J Pro 231(3):548–554. https://doi.org/10.1177/0954408915614300

3. Engbert T, Heymann T, Biermann D, Zabel A (2011) Flow drilling and thread forming of continuously reinforced aluminium extrusions. P I Mech Eng E-J Eng 225:398–407

4. Ramsay JMG (2008) Fliesslochformen und Gewindefurchen in dünne Bleche und Rohre aus Kupfer und Kupferlegierungen. Inauguraldissertation, Universität Kassel

5. Gopal Krishna PV, Kishore K, Satyanarayana V (2010) Some investigations in friction drilling AA6351 using high speed steel tools. ARPN. J Eng Appl Sci 5:11–15

6. Prabhu T, Arulmurugu A (2014) Experimental an analysis of friction drilling on Aluminium and copper. IJMET 5:130–139

7. Ozek C, Demir Z (2013) Investigate the friction drilling of aluminium alloys according to the thermal conductivity. Tem J 2:93–101

8.   Miller SF, Blau PJ, Shih AJ (2005) Microstructural alterations associated with friction drilling of steel, aluminum, and titanium. J Mater Eng Perform 14(5):647–653. https://doi.org/10.1361/105994905X64558

9.   Boopathi M, Shankar S, Manikandakumar S, Ramesh R (2013) Experimental investigation of friction drilling on brass, aluminium and stainless steel. Process Eng 64:1219–1226. https://doi.org/10.1016/j.proeng.2013.09.201

10. Gopichand A, Brahmam MV, Bhanuprakash D (2014) Experimental investigations and multi-objective optimization of friction drilling process on AISI 1015. IJAER 3

11. Nagarajan HN, Kotrappa H, Mallanna C, Venkatesh VC (1981) Mechanics of flow forming. CIRP Ann Manuf Technol 30(1): 159–162. https://doi.org/10.1016/S0007-8506(07)60915-9

12. Hirsch J (2011) Aluminium in innovative light-weight car design. Mater Trans 52(5):818–824. https://doi.org/10.2320/matertrans.L-MZ201132

13. Wittke P, Cyclic WF (2016) Deformation behavior of friction drilled internal threads in AlSi10Mg and AZ31 profiles. Procedia Struct. Integrity 2:3264–3271. https://doi.org/10.1016/j.prostr.2016.06.407

14. Krauß M (2007) Zur thermischen Ermüdung der Magnesiumbasislegierungen AZ31 und AZ91. Dissertation, University Kassel

15. Oezkaya E (2016) FEM-basiertes Softwaresystem für die effiziente 3D-Gewindebohrsimulation und Werkzeugoptimierung mittels CFD-Simulation. Vulkan, Essen

16. Ucun İ, Aslantas K, Oezkaya E, Cicek A (2017) 3D numerical modelling of micro-milling process of Ti6Al4V alloy and experimental validation. Int J Adv Manuf Tech 3(3):250–260. https://doi.org/10.1080/2374068X.2016.1247343

17. Zabel A (2016) Prozesssimulation in der Zerspanung – Modellierung von Dreh- und Fräsprozessen. Vulkan, Essen

18. Dehghan S, Ismail MIS, Ariffin MKA, Baharudin BT, Sulaiman S (2017) Numerical simulation on friction drilling of aluminum alloy. Mater Werkst 48(3-4):241–248. https://doi.org/10.1002/mawe.201600768

19. Danish M, Ginta TL, Wahjoedi BA (2016) Enhanced functional properties of mg alloys by cryogenic machining. IJAER I 11: 5055–5059

20. Hutchinsona B, Barnett MR, Ghaderi A, Cizek P, Sabirov I (2009) Deformation modes and anisotropy in magnesium alloy AZ31. Int J Mater Res 100(4):556–563

21. Ostermann F (2014) Anwendungstechnologie Aluminium. Springer, Berlin Heidelberg